

Detecting the First Stars and Black Holes with 21-cm Cosmology

RENNAN BARKANA¹

*Raymond and Beverly Sackler School of Physics and Astronomy
Tel Aviv University, Tel Aviv 69978, Israel*

Understanding the formation and evolution of the first stars and galaxies represents one of the most exciting frontiers in astronomy. Since the universe was filled with neutral hydrogen at early times, the most promising method for observing the epoch of the first stars is using the prominent 21-cm spectral line of the hydrogen atom. Current observational efforts are focused on the reionization era (cosmic age $t \sim 500$ Myr), with earlier times considered much more challenging. However, the next frontier of even earlier galaxy formation ($t \sim 200$ Myr) is emerging as a promising observational target. This is made possible by a recently noticed effect of a significant relative velocity between the baryons and dark matter at early times. The velocity difference significantly suppresses star formation. The spatial variation of this suppression enhances large-scale clustering and produces a prominent cosmic web on 100 comoving Mpc scales in the 21-cm intensity distribution. This structure makes it much more feasible for radio astronomers to detect these early stars, and should drive a new focus on this era, which is rich with little-explored astrophysics.

PRESENTED AT

The 10th International Symposium on Cosmology and
Particle Astrophysics (CosPA2013)
Honolulu, Hawaii, U.S.A., November 12–15, 2013

¹This work was supported by Israel Science Foundation grant 823/09 and the Ministry of Science and Technology, Israel.

1 Introduction

Galaxies around us have been mapped systematically out to a redshift $z \sim 0.3$ by recent large surveys. The observed galaxy distribution shows a large-scale filament-dominated “cosmic web” pattern that is reproduced by cosmological numerical simulations. This structure is well-understood theoretically as arising from the distribution of the primordial density fluctuations, which drove hierarchical structure formation in the early universe. Recent observations have been pushing a new frontier of early cosmic epochs, with individual bright galaxies detected reliably from as early as $z = 7.2$ [1], which corresponds to $t \sim 750$ Myr after the Big Bang.

The best hope of observing the bulk population of early stars is via the cosmic radiation fields that they produced. In particular, this radiation affected the hyperfine spin-flip transition of neutral hydrogen (H I) at a wavelength of 21 cm, potentially the most promising probe of the gas and stars at early times. Observations of this line at a wavelength of $21 \times (1 + z)$ cm can be used to slice the universe as a function of redshift z and obtain a three-dimensional map of the diffuse H I distribution within it [2], in the previously unexplored era of redshifts $\sim 7 - 200$. See Figure 1 for a brief summary of early cosmic history.

A major goal of current and upcoming observations is to probe the era of cosmic reionization. Ever since the discovery that the intergalactic gas throughout the Universe is highly ionized, astronomers have been searching for the period when the hydrogen was ionized for a second time after it became neutral at cosmic recombination. This reionization is the most recent cosmic phase transition, whereby the gas was ionized throughout the Universe, affecting subsequent galaxy formation and potentially detectable through its effect on a large range of observations.

In 2004 we argued [4] that the typical sizes of H II bubbles during reionization should be around 10 or 20 Mpc (see Figure 2), while many numerical simulations of reionization at the time followed a total volume below this size. Further analytical models [9] and large-scale numerical simulations [5, 6, 7, 8] have indeed demonstrated the dominance of large bubbles due to large groups of strongly-clustered galaxies. This has helped motivate the large number of observational efforts currently underway, since large-scale fluctuations are easier to detect (as they do not require high angular resolution).

Several arrays of low-frequency radio telescopes are currently being constructed in order to detect the 21-cm fluctuations from cosmic reionization. Current efforts include the Murchison Wide-field Array (MWA), the Low Frequency Array (LOFAR), the Giant Metrewave Radio Telescope (GMRT), and the Precision Array to Probe the Epoch of Reionization (PAPER); plans have been made for a future Square Kilometer Array (SKA).

In 2005 we showed [10] that fluctuations in the galaxy number density cause fluctuations even in the intensity of long-range radiation, leading to promising sources

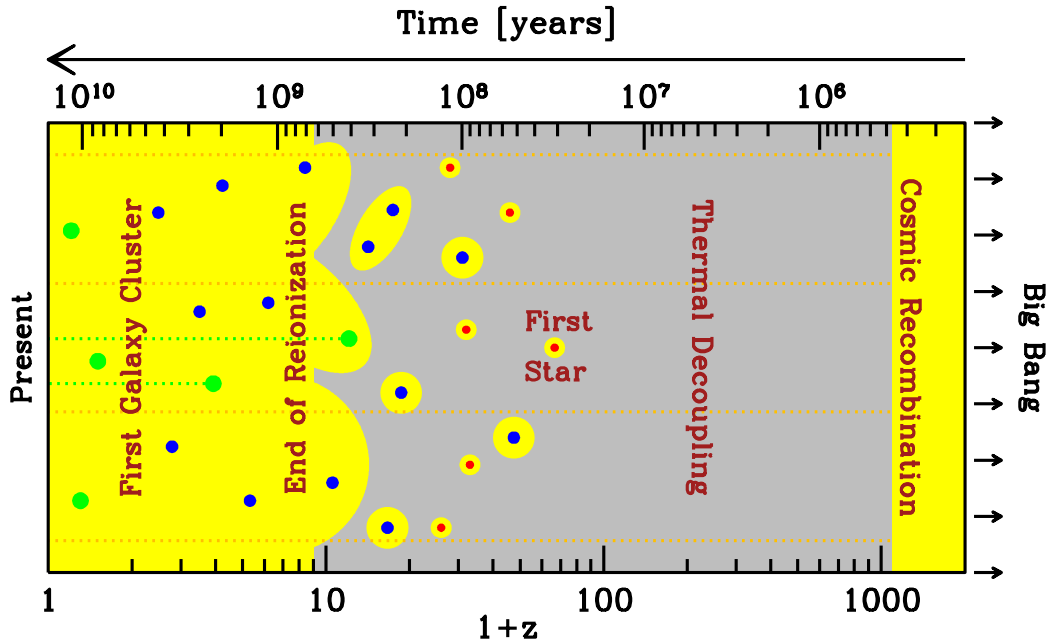


Figure 1: Overview of cosmic history, with the age of the universe shown on the top axis and the corresponding redshift on the bottom axis. Yellow represents ionized hydrogen, and gray is neutral. Observers probe the cosmic gas using the absorption of background light (dotted lines) by atomic hydrogen. Stars formed in halos whose typical size continually grew with time, going from the first generation that formed through molecular-hydrogen cooling (red dots), to the larger galaxies that formed through atomic cooling and likely dominated cosmic reionization (blue dots), all the way to galaxies as massive as the Milky Way, some of which host bright quasars (green dots). From [3].

of 21-cm fluctuations at even higher redshifts. Specifically, the 21-cm emission at high redshift is affected by $\text{Ly}\alpha$ radiation from stars and X-ray radiation from stellar remnants (mostly X-ray emitting black-hole binaries) [11]. We considered fluctuations in the $\text{Ly}\alpha$ radiation that helps maintain the 21-cm signal. Similar (though somewhat larger and later) fluctuations are expected from heating due to an inhomogeneous X-ray background [12].

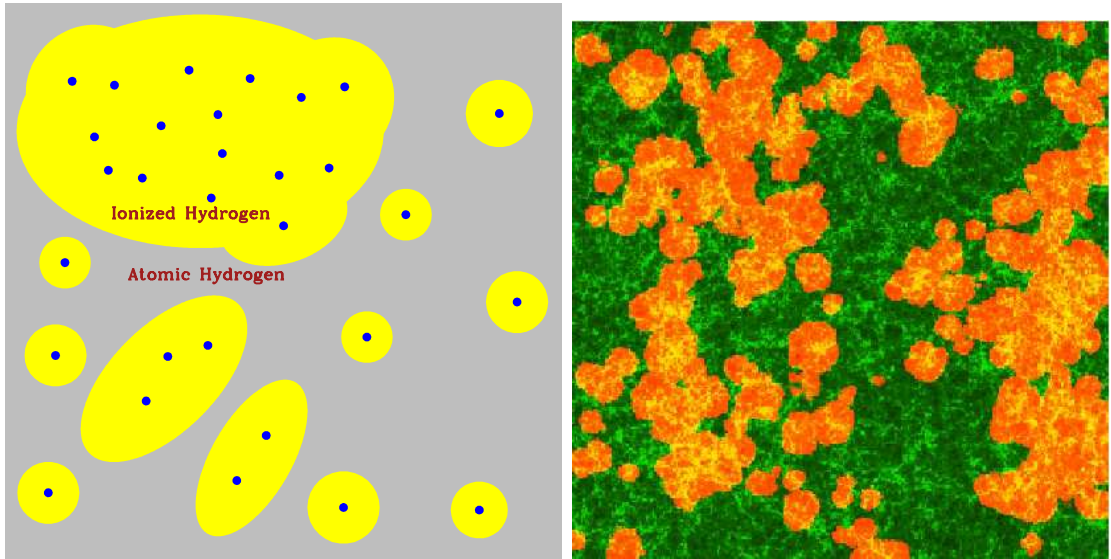


Figure 2: During reionization, the ionized bubbles created by clustered groups of galaxies [4] imprinted a signature in the power spectrum of 21-cm fluctuations [9]. The illustration (left panel, from [3]) shows how regions with large-scale overdensities form large concentrations of galaxies (dots) whose ionizing photons produce large ionized bubbles. At the same time, other large regions have a low density of galaxies and are still mostly neutral. A similar pattern has been confirmed in large-scale numerical simulations of reionization (right panel, showing a two-dimensional slice from a 150 Mpc simulation box [7]).

2 The streaming velocity: relative motion between the baryons and dark matter

Up until recently, studies of early structure formation were based on initial conditions from linear perturbation theory. However, there is an important effect missing from this treatment [13]. At early times, the electrons in the ionized gas scattered strongly with the then-energetic CMB photons, so that the baryons moved together with the photons in a strongly-coupled fluid. On the other hand, the motion of the dark matter was determined by gravity, as it did not otherwise interact with the photons. Thus, the initial inhomogeneities in the universe led to the gas and dark matter having different velocities. The key properties of this relative motion is that the velocity is generated by large-scale modes, and that it contains a strong baryon acoustic oscillation (BAO) signature.

The streaming velocity has a major effect on the first stars, since it suppresses the abundance of halos [13], suppresses the gas content of halos [14], and increases the minimum mass of halos in which stars can form from gas that cools via molecular

hydrogen cooling [16, 17, 18]. Many small-scale numerical simulations have studied this [19, 20, 21, 22, 23] (see Figure 3).

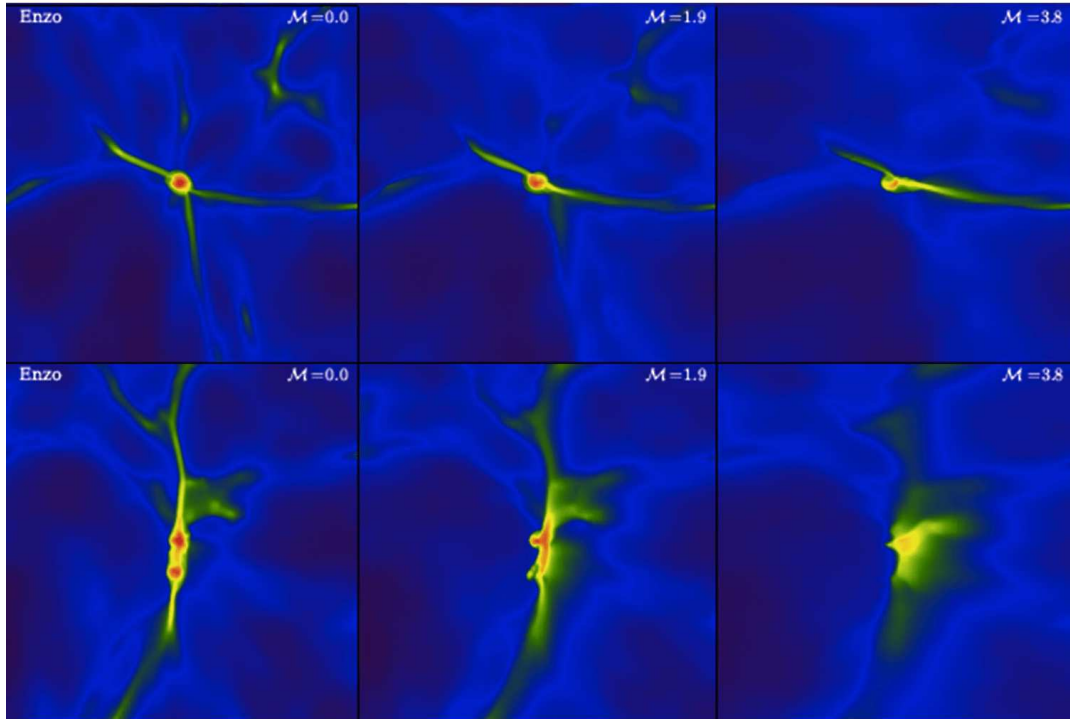


Figure 3: Effect of relative velocity on individual halos, from numerical simulations (including gravity and hydrodynamics). The colors indicate the gas density, which ranges from 10^{-26}g/cm^3 (blue) to 10^{-23}g/cm^3 (red). Two halos are shown at $z = 20$, with a total halo mass of $2 \times 10^6 M_\odot$ (top) or $8 \times 10^5 M_\odot$ (bottom). Panels show the result for gas initially moving to the right with a relative velocity of 0 (left), 1 (middle), or 2 (right) in units of the root-mean-square value of the relative velocity at $z = 20$. \mathcal{M} indicates the corresponding Mach number at $z = 20$. From [20].

3 Detecting the first stars at redshift 20

Full numerical simulations that successfully resolve the mini-galaxies that hosted the first stars are limited to ~ 1 Mpc volumes. On the other hand, only large cosmological scales are accessible to 21-cm observations (which are currently limited to low angular resolution). Purely analytical calculations typically require simplifying assumptions and thus achieve limited accuracy. Thus, the best way to generate

observable predictions from the era of early galaxies is with a hybrid method that combines linear theory on large scales with the results of numerical simulations on small scales. We recently developed such a hybrid method and used it to produce the first realistic, three-dimensional images of the expected large-scale distribution of the first stars and the resulting 21-cm emission [24]. In our approach we built upon previous hybrid methods used for high-redshift galaxy formation [13, 14, 15].

Velocities are coherent on larger scales than the density (Figure 4). The resulting distribution of stellar density at $z = 20$ is shown in Figure 5. The velocity effect produces a more prominent cosmic web on large scales, marked by large coherent regions that have a low density of stars, separated by ribbons or filaments of high star formation. The effect is even stronger at higher redshifts, which substantially alters the feedback environment of the first stars.

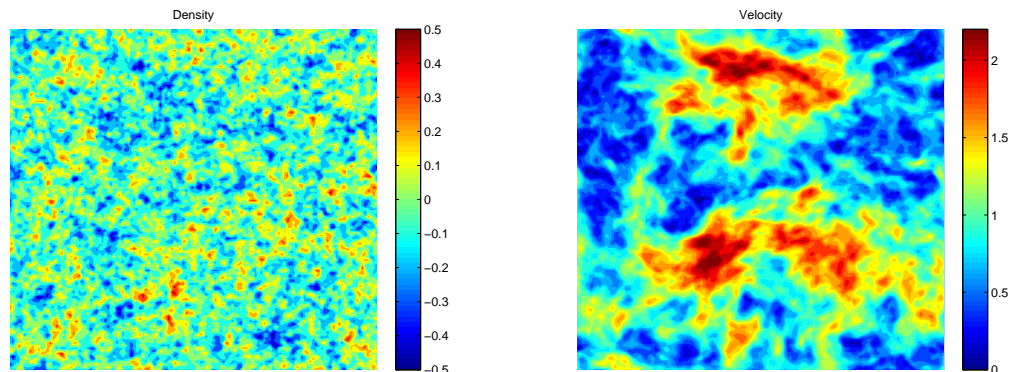


Figure 4: The large-scale density and velocity fields in an example of a slice from a simulated volume 384 Mpc on a side (based on [24], but taken from a different box from the one shown in the Figures in [24], i.e., for a different set of random initial conditions). The thickness of the slice is 3 Mpc (which is also the pixel size of our grid). For the density field (left panel), we show the fractional perturbation relative to the mean, at $z = 20$; for the velocity field (right), we show the magnitude of the relative motion in units of the root-mean-square value (the map is independent of redshift in these relative units).

Observationally, these degree-scale fluctuations will affect various cosmic radiation backgrounds, and in particular the history of 21-cm emission and absorption. We focus here on heating fluctuations, which are maximized roughly at the heating transition (when the cosmic mean gas temperature equals that of the cosmic microwave background (CMB)). Figure 6 shows the gas temperature distribution at $z = 20$ (assuming the heating transition occurs at that time). Regions where the gas moved rapidly with respect to the dark matter (dark red regions, right panel of Figure 4) produced fewer stars (dark blue regions, right panel of Figure 5) and thus

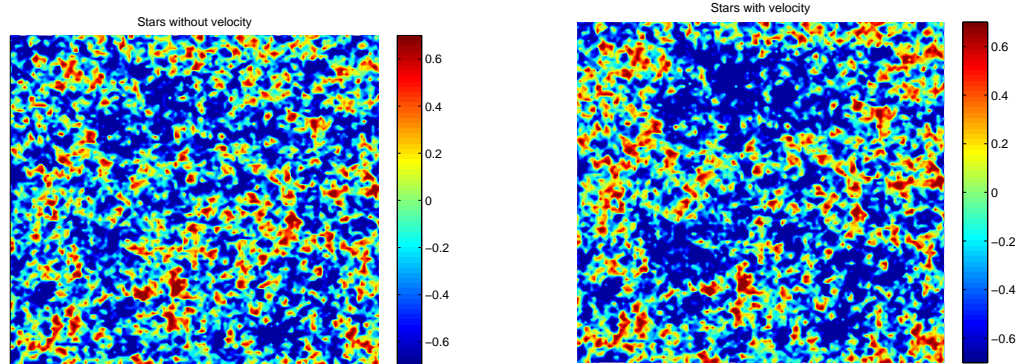


Figure 5: Effect of relative velocity on the number density of stars at redshift 20. For the same slice as in Figure 4, we compare the previous expectation (left panel), including the effect of density only, to the new prediction (right), including the effect of the same density field plus that of the relative velocity. The colors correspond to the logarithm of the gas fraction in stars, in units of its cosmic mean value in each case.

a lower X-ray intensity, leaving large regions with gas that is still colder than the CMB by a factor of several (dark blue regions, right panel of Figure 6). The large voids in star formation produced by a high relative velocity lead to prominent 21-cm absorption (dark blue regions, right panel of Figure 7) seen on top of the pattern from the effect of density fluctuations. These deep 21-cm cold spots are the main observable signature of the effect of the relative velocity on the first stars.

While these Figures illustrate the detailed pattern resulting from the effect of relative velocity on the 21-cm intensity distribution, upcoming experiments are expected to yield very noisy maps that likely must be analyzed statistically. Figure 8 shows the predicted effect on a key statistic, the power spectrum of the fluctuations in 21-cm intensity (from [24]). The velocities enhance large-scale fluctuations (blue solid curve compared with red dotted), leading to a flatter power spectrum with prominent baryon acoustic oscillations. The signal is potentially observable with a redshift 20 version of current instruments (green dashed curve). At even higher redshifts, the fluctuations imprinted by the inhomogeneous Ly α background in the 21-cm signal at $z \sim 25$ should be detectable with the Square Kilometer Array (Figure 9).

ACKNOWLEDGEMENTS

I thank my collaborators on the cited work: Anastasia Fialkov, Eli Visbal, Arazi Pinhas, Dmitriy Tselikhovich, Chris Hirata, Avi Loeb, and Smadar Naoz. (See grant acknowledgements at bottom of cover page)

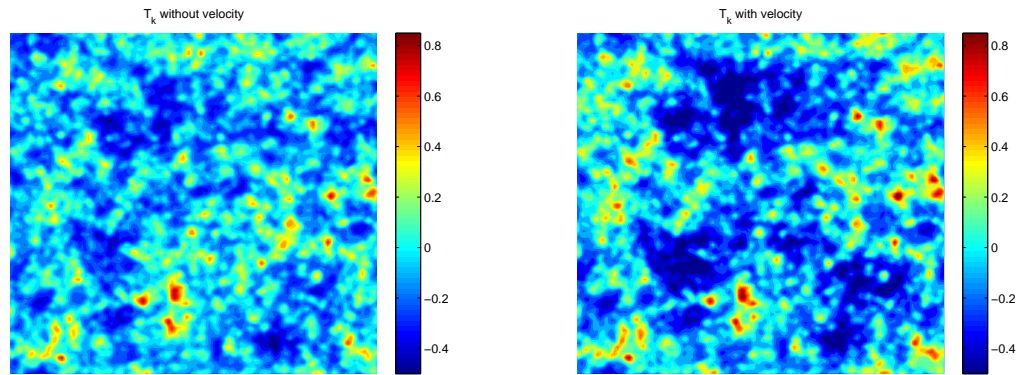


Figure 6: Effect of relative velocity on the gas temperature at redshift 20. For the same slice as in Figure 4, we compare the previous expectation (left panel) to the new prediction (right), which includes the effect of relative velocity. The colors correspond to log of the gas (kinetic) temperature in units of the CMB temperature at $z = 20$.

References

- [1] Ono, Y. et al. 2012, ApJ, 744, 83
- [2] Hogan, C. J., & Rees, M. J. 1979, MNRAS, 188, 791
- [3] Barkana, R. 2006b, Science, 313, 931
- [4] Barkana R., & Loeb A. 2004, ApJ, 609, 474
- [5] Ciardi B., Ferrara A., & White S. D. M. 2003, MNRAS, 344, L7
- [6] Zahn O., Lidz A., McQuinn M., Dutta S., Hernquist L., Zaldarriaga M., Furlanetto S. R., 2007, ApJ, 654, 12
- [7] Mellema G., Iliev I. T., Pen U.-L., Shapiro P. R., 2006, MNRAS, 372, 679
- [8] Santos MG, Amblard A, Pritchard J, Trac H, Cen R, Cooray A 2008, ApJ, 689, 1
- [9] Furlanetto S. R., Zaldarriaga M., Hernquist L., 2004a, ApJ, 613, 1
- [10] Barkana, R., & Loeb, A. 2005b, ApJ, 626, 1
- [11] Madau, Meiksin, & Rees 1997, ApJ, 475, 429
- [12] Pritchard, J. R., Furlanetto, S. R. 2007, MNRAS, 376, 1680
- [13] Tseliakhovich D., Hirata C. M., 2010, PRD, 82, 083520

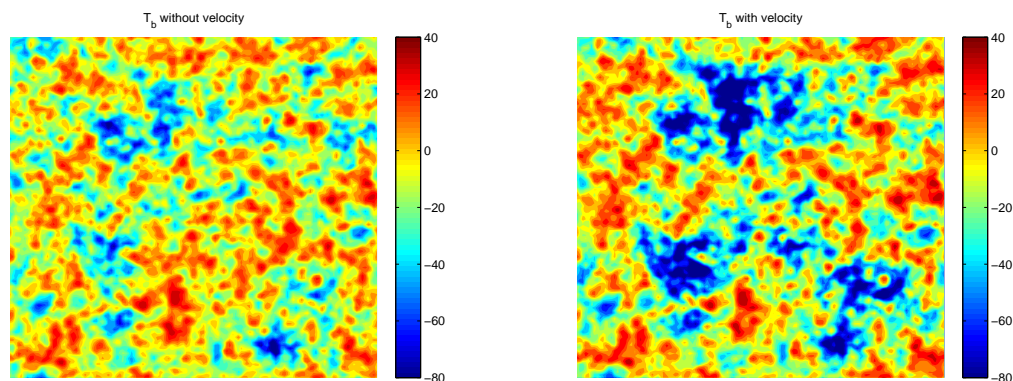


Figure 7: Effect of relative velocity on the $z = 20$ 21-cm brightness temperature (which measures the observed intensity of radio waves emitted by intergalactic hydrogen). For the same slice as in Figure 4, we compare the previous expectation (left panel) to the new prediction (right), which includes the effect of relative velocity. The colors correspond to the 21-cm brightness temperature in millikelvin units.

- [14] Dalal N., Pen U.-L., Seljak U., 2010, JCAP, 11, 7
- [15] Mesinger, A., Furlanetto, S., Cen, R., 2011, MNRAS, 411, 955
- [16] Stacy A., Bromm V., Loeb A., 2012, MNRAS, 413, 543
- [17] Greif, T., White, S., Klessen, R., & Springel, V., 2011, ApJ, 736, 147
- [18] Fialkov, A., Barkana, R., Tseliakhovich, D., Hirata, C. 2012, MNRAS, 424, 1335
- [19] Maio, U., Koopmans, L. V. E., Ciardi, B. 2011, MNRAS, 412, L40
- [20] O’Leary, R. M., & McQuinn, M. 2012, ApJ, 760, 4
- [21] McQuinn, M., & O’Leary, R. M. 2012, ApJ, 760, 3
- [22] Naoz, S., Yoshida, N., & Gnedin, N. Y. 2012, ApJ, 747, 128
- [23] Naoz, S., Yoshida, N., & Gnedin, N. Y. 2013, ApJ, 763, 27
- [24] Visbal, E., Barkana, R., Fialkov, A., Tseliakhovich, D., & Hirata, C. M. 2012, Nature, 487, 70
- [25] McQuinn, M., Zahn, O., Zaldarriaga, M., Hernquist, L., & Furlanetto, S. R. 2006, ApJ, 653, 815
- [26] Fialkov, A., Barkana, R., Pinhas, A., & Visbal, E. 2014, MNRAS, 437, L36

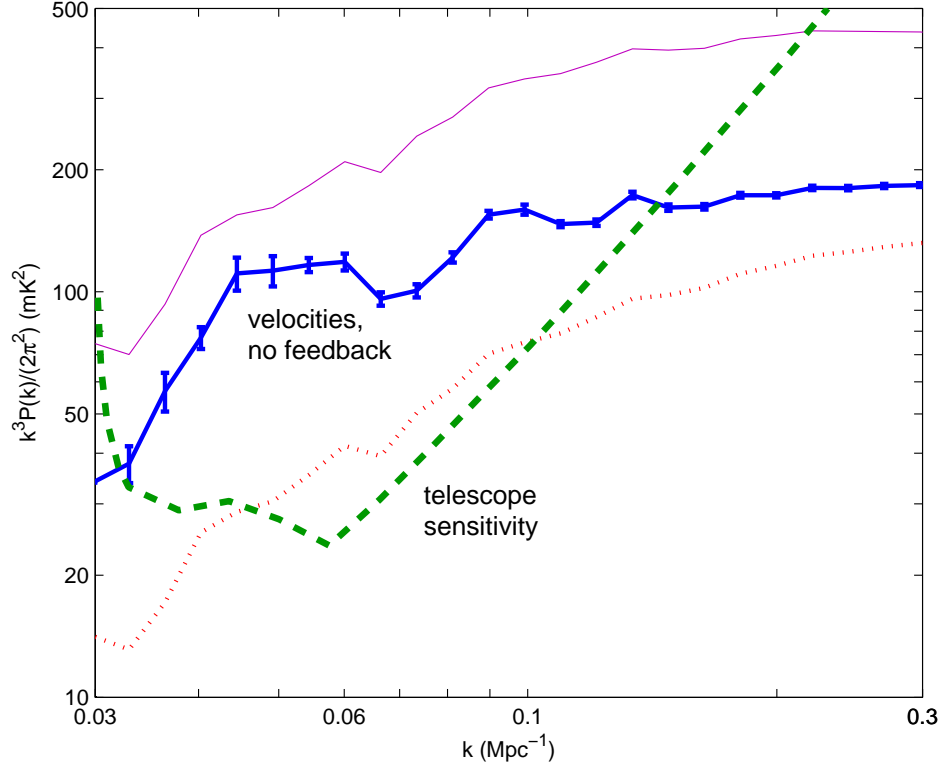


Figure 8: Signature of the relative velocity in the 21-cm power spectrum, at the peak of the X-ray heating transition at $z = 20$. We consider the prediction including the relative velocity effect (blue solid curve) or with the effect of densities only (red dotted curve). These predictions are compared to the projected $1\text{-}\sigma$ telescope sensitivity (green dashed curve) based on 1000-hour observations with an instrument like the MWA or LOFAR but designed to operate at 50–100 MHz [25]. Future experiments like the Square Kilometer Array should reach a better sensitivity than this by more than an order of magnitude. To allow for the possibility of feedback, we also show the prediction for the case where star formation requires atomic cooling (purple solid curve). In this plot we have fixed the heating transition at $z = 20$ for easy comparison among the various cases. From [24].

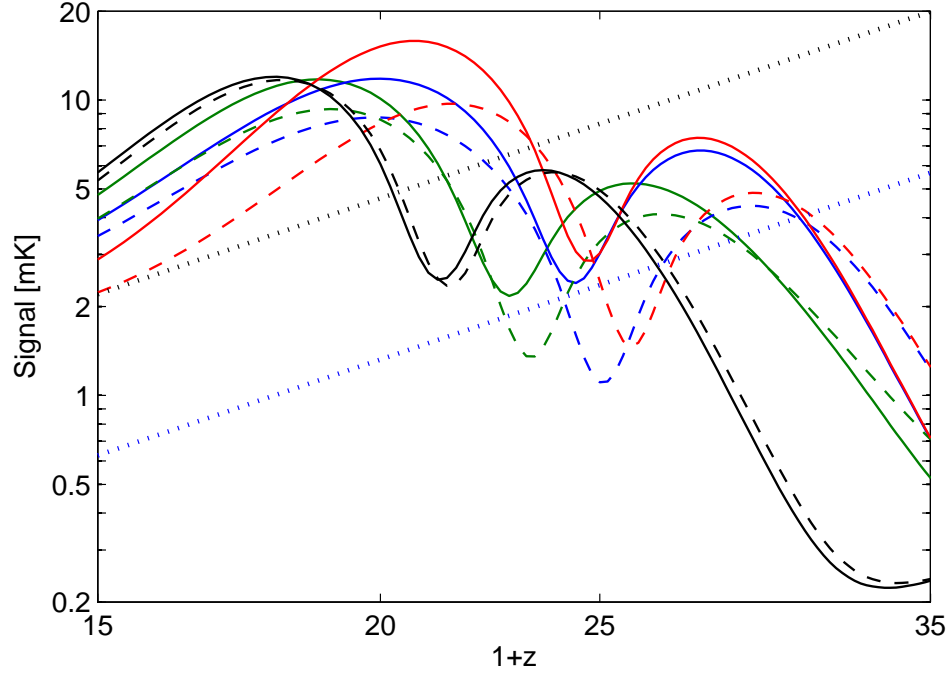


Figure 9: Amplitude of the 21-cm brightness temperature at 125 Mpc, the BAO scale. We show the signal with (solid) and without (dashed) the streaming velocity for no H_2 cooling (black), strong (green) and weak (blue) feedback and for no feedback (red). We also show the sensitivity curves for SKA (blue dotted) and MWA/LOFAR-like (black dotted) experiments; the latter refers to an instrument with the same collecting area as MWA or LOFAR, and the former to the planned SKA, where to both we have applied an estimated degradation factor due to foreground removal (see [25] and [24] for details). From [26]